CHEMISTRY
A EUROPEAN JOURNAL

DOI: 10.1002/chem.200800639

A Universal Model for Nanoporous Carbon Supercapacitors Applicable to Diverse Pore Regimes, Carbon Materials, and Electrolytes

Jingsong Huang,* Bobby G. Sumpter, and Vincent Meunier[a]

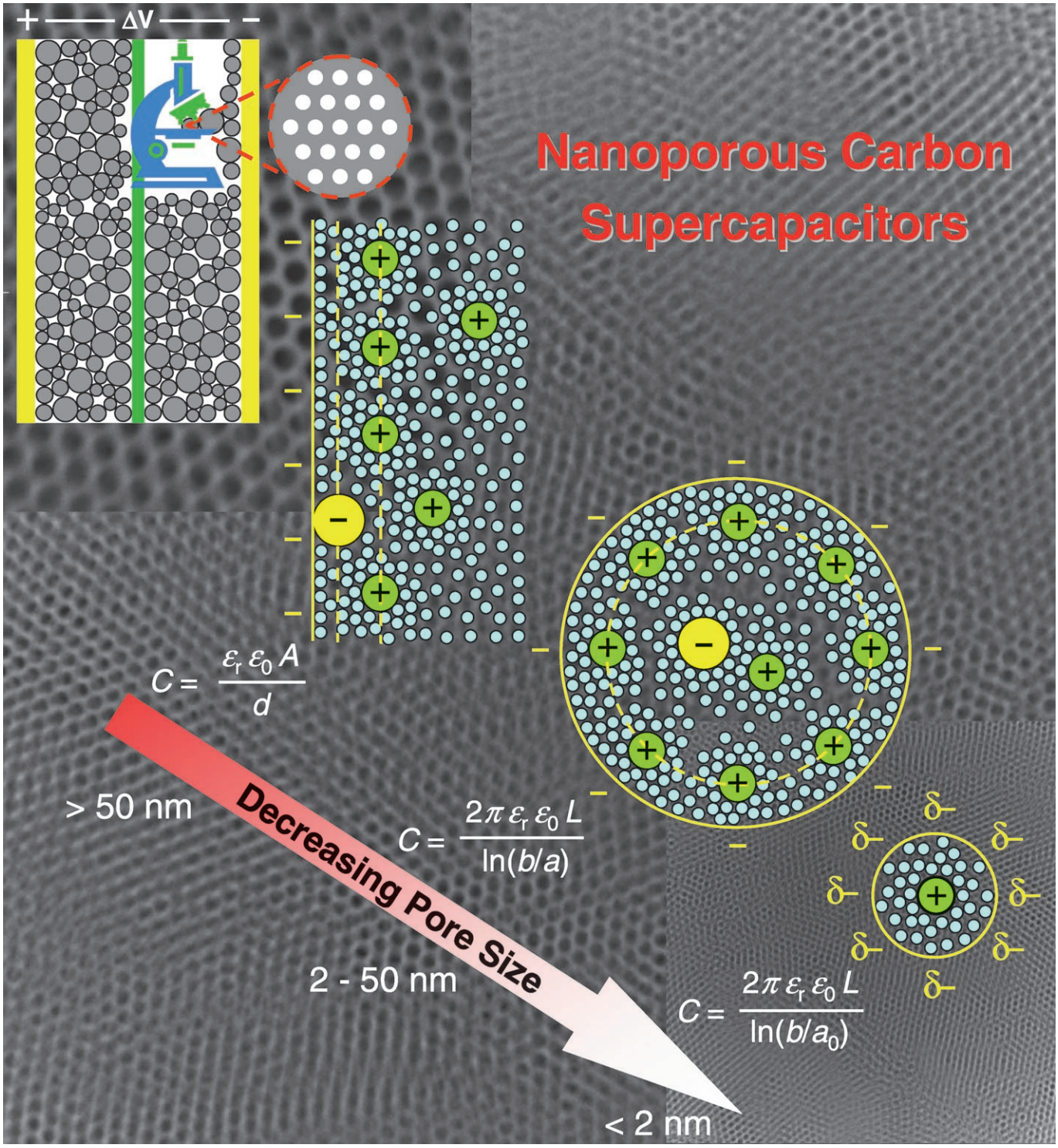

Abstract: Supercapacitors, commonly called electric double-layer capacitors (EDLCs), are emerging as a novel type of energy-storage device with the potential to substitute batteries in applications that require high power densities. In response to the latest experimental breakthrough in nanoporous carbon supercapacitors, we propose a heuristic theoretical model that takes pore curvature into account as a replacement for the EDLC model, which is based on a traditional parallel-plate capacitor. When the pore size is in the mesopore regime (2–50 nm), counterions enter mesoporous carbon materials and approach the pore wall to form an electric double-cylinder capacitor (EDCC); in the micropore regime (<2 nm), solvated/desolvated counterions line up along the pore axis to form an electric wire-in-cylinder capacitor (EWCC). In the macropore regime (>50 nm) at which pores are large enough so that pore curvature is no longer significant, the EDCC model can be reduced naturally to the EDLC model. We present density functional theory calculations and detailed analyses of available experimental data in various pore regimes, which show the significant effects of pore curvature on the supercapacitor properties of nanoporous carbon materials. It is shown that the EDCC/EWCC model is universal for carbon supercapacitors with diverse carbon materials, including activated carbon materials, template carbon materials, and novel carbide-derived carbon materials, and with diverse electrolytes, including organic electrolytes, such as tetraethylammonium tetrafluoroborate ($TEABF_4$) and tetraethylammonium methylsulfonate (TEAMS) in acetonitrile, aqueous H_2SO_4 and KOH electrolytes, and even an ionic liquid electrolyte, such as 1-ethyl-3-methylimidazolium bis(trifluoromethanesulfonyl)imide (EMI-TFSI). The EDCC/EWCC model allows the supercapacitor properties to be correlated with pore size, specific surface area, Debye length, electrolyte concentration and dielectric constant, and solute ion size It may lend support for the systematic optimization of the properties of carbon supercapacitors through experiments. On the basis of the insight obtained from the new model, we also discuss the effects of the kinetic solvation/desolvation process, multimodal (versus unimodal) pore size distribution, and exohedral (versus endohedral) capacitors on the electrochemical properties of supercapacitors.

Keywords: carbon · density functional calculations · electric double layer · mesoporous materials · supercapacitors

Introduction

Supercapacitors, commonly called electric double-layer capacitors (EDLCs), bridge the gap between batteries and conventional dielectric capacitors, and are ideal for the rapid storage and release of energy.[1,2] Supercapacitors have a much higher energy density than conventional dielectric capacitors due to the large surface area of porous electrode materials; they also have a higher power density and a longer lifetime than batteries due to the absence of Faradaic processes in the electric double layer.[3] Current trends in supercapacitor research include the development of nanoporous carbon materials for supercapacitor electrode materials owing to the high surface area, high conductivity, and relatively low cost of carbon materials.[4] Supercapacitors based on nanoporous carbon materials have recently attracted considerable attention as novel energy-storage devices.[4–6] This paper is concerned with various nanoporous carbon materials suitable for supercapacitors, including activated carbon materials, template carbon materials, and, in particular, novel carbide-derived carbon (CDC) materials.[7]

[a] Dr. J. Huang, Dr. B. G. Sumpter, Dr. V. Meunier
Oak Ridge National Laboratory
Oak Ridge, TN 37831-6367 (USA)
Fax: (+1) 865-574-0680
E-mail: huangj3@ornl.gov

Supporting information for this article is available on the WWW under http://www.chemeurj.org/ or from the author.

Supercapacitors store energy by charge separation in an electric double layer formed at the electrode/electrolyte interface, in much the same way as conventional dielectric capacitors. The double layer at the electrode surface can form and relax almost instantaneously. Unlike batteries, this process involves no chemical reaction, thus allowing the rapid storage and release of energy. Generally it is assumed that the capacitance of supercapacitors follows that of a parallel-plate capacitor, as shown in Equation (1):[2b,c,4,6a]

$$C = \frac{\varepsilon_r \varepsilon_0 A}{d} \tag{1a}$$

$$C/A = \frac{\varepsilon_r \varepsilon_0}{d} \tag{1b}$$

in which ε_r is the electrolyte dielectric constant, ε_0 is the permittivity of a vacuum, A is the electrode specific surface area, and d is the effective thickness of the electric double layer (the Debye length). The Debye length is in the order of molecular dimensions, and carbon materials typically have specific surface areas up to $3000\,m^2g^{-1}$. With the capacitance being proportional to a very large A and being inversely proportional to a very small d, the energy density of supercapacitors is much higher than that of conventional dielectric capacitors.

To develop supercapacitors as an alternative to batteries, worldwide research efforts are currently aiming at increasing the energy density by optimizing the pore size distribution

of nanoporous carbon materials. In their breakthrough work, Gogotsi and co-workers[8] synthesized carbide-derived carbon materials with unimodal micropores[9] smaller than 1 nm. They found that these new materials exhibit an anomalous increase of capacitance in an organic electrolyte of acetonitrile compared with other carbon materials with pore sizes above 2 nm in which there is a slightly increased capacitance with increasing pore size. These results challenge the long-held presumption that pores smaller than the size of solvated electrolyte ions do not contribute to energy storage. Such anomalous increase in capacitance in subnanometer pores is ascribed to the desolvation of the electrolyte ions entering subnanometer pores,[8,10] which is verified by a recent experiment utilizing an ionic liquid electrolyte with no solvation shell around the electrolyte ions.[11] With a detailed literature survey, we found that this anomalous phenomenon is not unique with organic or ionic liquid electrolytes and CDCs, and it also manifests in aqueous solutions and in carbon materials other than CDCs. These new experimental discoveries pose an opportunity to further optimize the capacitance of carbon supercapacitors, together with a challenge for theory to rationalize the unusual experimental results.

The theoretical model based on Equation (1) has been used for EDLCs for decades and appears to be the first choice for the analysis of experimental results. Assuming a planar pore surface, Gogotsi and co-workers[8] found that the normalized capacitance of the micropores (C/A) is proportional to the reciprocal radius of the micropores ($1/d$). (In the analysis, the micropore radius was treated as the estimated double-layer thickness (d) shown in Equation (1).) This relationship follows Equation (1) quite well, which shows the dominance of the $1/d$ term relative to the effects of dielectric permittivity and pore curvature. However, close inspection reveals that the intercept of the linear fit is not zero,[12] which indicates there are some other effects that Equation (1) does not include. With more and more experimental data available in this field, scientists are gradually realizing that the parallel-plate capacitor model is insufficient for rationalizing the electrochemical properties of nanoporous carbon supercapacitors. Generally, it is expected, and indeed observed, that higher capacitances are obtained for carbon materials with higher surface areas, and some experiments indicate a linear relationship between C and A.[13] However, in some other experiments, it has been found that there is no such linear relationship.[14,15] There are also some experiments showing that there is a linear relationship between C and micropore volume.[16,17] The effects of pore size and d on C are also not clear. Traditional belief is that subnanometer pores may not be accessible to the electrolyte solution, simply because the electrolyte ions with solvation shells are too big to enter the pores; in contrast, new experiments point to a role played by the desolvated ions in subnanometer pores.[8,16,17] What happens inside the nanoconfined space within the pores is not fully understood.

Motivated by the recent new developments of nanoporous carbon supercapacitors and the lack of a good theoretical model in the field, herein we present a heuristic model for nanoporous carbon supercapacitors with the pore curvature taken into account. We show that, with this new model, one can explain the anomalous increase in capacitance for pores below 1 nm and the slightly increasing capacitance with increasing pore size above 2 nm. It can be reduced to the traditional parallel-plate capacitor model in Equation (1) for macropores of pore size >50 nm. The new model is applicable to diverse carbon materials, including activated carbon materials, template carbon materials, and CDCs in organic, aqueous, and even ionic liquid electrolytes. The parameters obtained from our analyses of the available experimental data using this model are in good agreement with experimental results and with our first-principles density functional theory (DFT) calculations.

Results and Discussion

Heuristic model: Herein, we limit our discussions to nanoporous carbon materials as active materials in the electrode films of supercapacitors. The grain size of carbon particles is in the order of micrometers. Each carbon particle contains a large amount of pores with diameters in the order of nanometers (Figure 1a). (According to IUPAC, nanoporous materials can be subdivided into three categories in terms of the pore sizes: micropores are less than 2 nm in diameter, mesopores are 2–50 nm in diameter, and macropores are larger than 50 nm in diameter.)[18] The large specific surface area of up to 3000 $m^2 g^{-1}$ includes a relatively small contribution from the surface area of the particles and a major contribution from the pores inside the particles. Simplification of the carbon/electrolyte interface to an EDLC (Figure 1b) does not consider the curvature of each pore, and accordingly, the close interactions between pore walls are neglected in the simple parallel-plate capacitor model. Equation (1) may

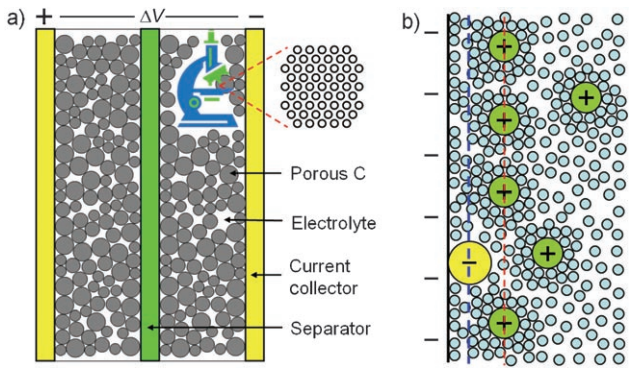

Figure 1. Schematic diagrams of a) a nanoporous carbon supercapacitor showing the construction of supercapacitors in which the porous carbon particles are approximated as balls and b) an electric double-layer capacitor (EDLC) formed at the carbon/electrolyte interface (anode) in which the inner and outer Helmholtz planes (IHP, OHP) are represented by blue and red dashed lines, respectively. Cations are shown to be solvated by the solvent molecules.

not reflect the actual scenario for mesopores and micropores. For macropores with a pore size above 50 nm, the electric double layer can be a good approximation for the carbon/electrolyte interface (see below).

Moving beyond the planar capacitor model, it seems reasonable to include the influence of pore curvature to describe the capacitance of carbon supercapacitors. Nanoporous materials can have various pore shapes, such as cylindrical, slit, and spherical types, depending on the synthesis approach.[19] Mesoporous carbon materials obtained by template methods usually have wormhole structures with cylindrical cross sections.[16,20] Cylindrical pores are generally the assumption for theoretical treatments for physical adsorption of gases[21] and impedance spectroscopy.[22] By assuming that the mesopores are cylindrical, solvated counterions enter pores and approach the pore walls to form electric double-cylinder capacitors (EDCCs; Figure 2a). The double-cylinder capacitance is given in Equation (2):[23]

$$C = \frac{2\pi\varepsilon_r\varepsilon_0 L}{\ln(b/a)} \tag{2a}$$

$$C/A = \frac{\varepsilon_r\varepsilon_0}{b\ln[b/(b-d)]} \tag{2b}$$

in which L is the pore length and b and a are the radii of the outer and inner cylinders, respectively.

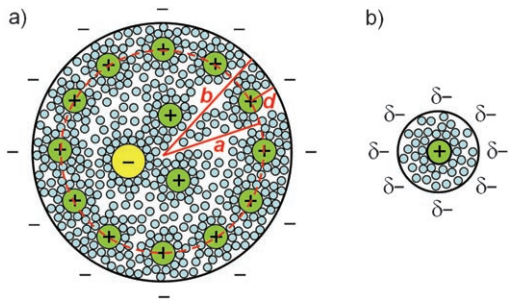

Figure 2. Schematic diagrams (top views) of a) a negatively charged mesopore with solvated cations approaching the pore wall to form an electric double-cylinder capacitor (EDCC) with radii b and a for the outer and inner cylinders, respectively, separated by a distance d, and b) a negatively charged micropore of radius b with solvated cations of radius a_0 lining up to form an electric wire-in-cylinder capacitor (EWCC). EWCC is also possible with desolvated ions (see text).

For micropores, however, the small pores do not allow the formation of a double cylinder. Assuming cylindrical micropores, solvated (or desolvated) counterions enter the pores and line up to form electric wire-in-cylinder capacitors (EWCCs; Figure 2b). Although the molecular geometries of the counterions might be anisotropic, the pore walls experience the average effect owing to the translation or room-temperature rotation of the counterions along or with respect to the pore axes, leading to an inner cylinder. Conversely, the counterions experience the average effect if the micropore shape is slightly distorted from a cylinder, leading to an outer cylinder. In a way, EWCCs can also be viewed as EDCCs, but the key quantity for EWCCs is no longer d, but rather the radius of the inner cylinder a_0, which is the effective size of the counterions (that is, the extent of electron density around the ions). By using a_0, Equation (2) then becomes Equation (3):

$$C/A = \frac{\varepsilon_r\varepsilon_0}{b\ln(b/a_0)} \tag{3}$$

Equations (2b) and (3) are used to fit the available experimental data for supercapacitors of nanoporous carbon materials with diverse pore sizes and electrolytes.[24]

Organic electrolytes: First we studied organic electrolytes, including tetraethylammonium tetrafluoroborate ($TEABF_4$) and tetraethylammonium methylsulfonate (TEAMS), dissolved in acetonitrile. The advantage of these organic electrolytes is the possibility of higher cell voltage, which results in higher stored energy per cell, than in aqueous electrolytes.

The experimental data shown in Figure 3 were scanned in from Figure 3 of reference [8], and were obtained from

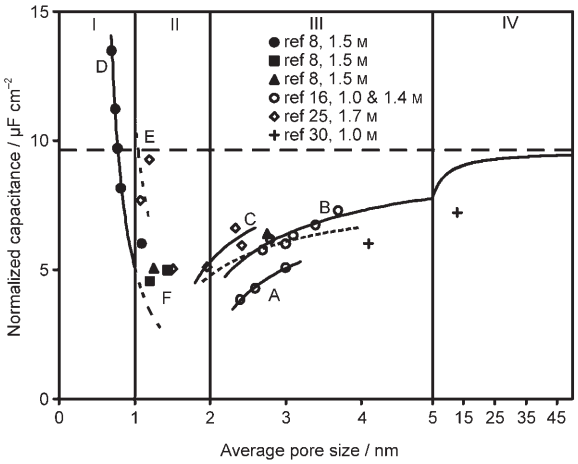

Figure 3. Experimental data from references [8], [16], and [25] were fitted by using Equation (2b) in region III and Equation (3) in region I; the extrapolation of the curve in region III into region IV approaches the broken line calculated by Equation (1b) with the same parameters as those obtained for region III. Data are divided into six groups (A–F) and a detailed analysis is described in the text. The dashed curve for group E is not a fitting result, but is shown as a visual guide.

Tables 2 and 3 of references [16] and [25], respectively. We also scanned the data for reference [16] from Figure 3 of reference [8] to compare with the data originally reported in Table 2 of reference [16]. We found that the scanned data have acceptable relative errors of $\leq 1\%$. For consistency, three data points from reference [25] were recalculated by using the specific surface area of the electrode instead of the powder. (The specific surface areas of electrodes are lower than those of corresponding powder materials due to the use of binding mixture.) The capacitances of microporous carbon materials are reduced at higher discharging cur-

rent densities. Herein we analyze the data obtained at a discharging current density of 5 mA cm^{-2}.[8] In comparison, the experiments described in references [16] and [25] were performed with a small voltammetric scan rate of 2 mV s^{-1} and a low discharging current density of 10 mA cm^{-2}.

First, we fit all of the mesoporous data in region III using Equation (2b), in which it is reasonable to approximate the pores as cylinders. The dashed curve reproduces the trend of slightly increasing capacitance with increasing pore size, albeit the goodness of fit (R^2) is only 0.259. The challenge to fit all data well comes from the different conditions employed in the three experiments. These carbon materials have contributions to capacitance from both micropores and mesopores;[16,25] and therefore, strictly speaking the pores are not unimodal. This hampers the application of one set of parameters in the theoretical model because our model is only applicable to unimodal pores and the fitting quality will be worse when applied to multimodal pores. In addition, the electrolyte in reference [25] is TEAMS in CH_3CN, whereas the electrolyte in references [8] and [16] is $TEABF_4$ in CH_3CN. Finally, the concentrations are different, ranging from 1.0,[16] 1.4,[16] and 1.5[8] to 1.7 M[25] (Figure 3, Table 1). To fit the experimental results well, it is necessary to subdivide the data to take into account the differences in experimental conditions. Noticing that the data for a concentration of 1.7 M is on the top, and the single data point for a concentration of 1.5 M is in the middle between 1.7 and 1.0 M, we break down the data to fit them by concentration. The data in reference [16] were obtained from 1.0 and 1.4 M $TEABF_4$ in CH_3CN, but the specific concentrations were not described.[6a,16] We tentatively assign group A to 1.0 M and group B to 1.4 M on the basis of the typical trend.[26] The only data point from reference [8] in region III is included in group B for analysis because 1.5 M is close to 1.4 M. These respective fittings produce much better R^2 values (Table 1).

As can be seen from Table 1, the d values are of the same order of magnitude as the calculated solvated ionic radii of $TEA^+ \cdot 7CH_3CN$ (6.5 Å) and $BF_4^- \cdot 9CH_3CN$ (5.8 Å),[27] and the Debye length of $TEABF_4$ in CH_3CN (6.6 Å), which was estimated from impedance spectroscopy.[26] One also notices the trend in Table 1 that d increases with decreasing concentration, showing the increasing effective Debye screening length with dilution.[26] The dielectric constant from the fitting is about 9, which is much smaller than the value of 36 for the bulk CH_3CN at room temperature.[28] However, it has been found that the dielectric constant of an aqueous solution decreases in electric double layers and confined spaces.[1,29] In addition, these data were obtained from diverse carbon materials, including activated carbon materials, template carbon materials, and CDCs. It appears that our proposed model is valid regardless of what carbon materials are used in the electrodes. The limited number of data points for groups A and C puts the significance of the fitting results into question, but we stress that the model describes the trend correctly not only for the data after it has been subdivided into three groups, but for the data as a whole group. Further experimental studies using various concentrations of one electrolyte solution are encouraged for carbon supercapacitors with narrow mesopore size distributions.

We supplement the three data points of group A with two capacitance values obtained with a voltammetric scan rate of 1 mV s^{-1} for two template mesoporous carbon materials in 1.0 M $TEABF_4$ in CH_3CN.[30] These data, together with those of group A, indicate that the trend of slightly increasing capacitance of mesoporous carbon materials with increasing pore size is valid for a wide pore range. The extrapolation of the curve for group B into region IV shows that the curve asymptotically approaches the broken line calculated by Equation (1b) using the same parameters, ε_r and d, as in group B. In fact, Equation (2b) for EDCCs can be reduced to Equation (1b) for EDLCs by using Taylor's expansion for large pores when $d \ll a$.[12] This result indicates that the curvature plays a significant role in the capacitance of mesopores, but not in that of macropores for which the carbon/electrolyte interface can be approximated by an electric double layer. The broken line represents the limiting value of normalized capacitance for large pores at a concentration of 1.5 M.

Going down in size to micropores, especially below 1 nm, we fit group D in region I with Equation (3), reproducing the anomalous increase in capacitance. The ε_r value of 2.23 is very close to the vacuum value of 1, which is reasonable because the space between counterions and pore walls is not an absolute vacuum, but has some finite electron density. This shows that the solvation shell of the counterions is completely removed, as suggested by Vix-Guterl et al.[16] The a_0 value of 2.30 Å will be addressed in the next section on the basis of DFT calculations on the radial charge distribution of TEA^+ and BF_4^-. Gogotsi and co-workers[8] also

Table 1. Fitting results for the experimental data in regions I and III of Figure 3 using Equations (3) and (2b), respectively. Depending on the various experimental conditions in references [8], [16], and [25], experimental data are subdivided into several groups for detailed analysis. Numbers in parentheses are standard errors of parameters.

Data group	Region	Electrode materials	Electrolyte	Concentration [M]	R^2	ε_r	d [Å]	a_0 [Å]
A[a]	III	template C	$TEABF_4$	1.0[b]	0.993	9.65 (0.51)	10.15 (0.02)	–
B[a]	III	template C and CDC	$TEABF_4$	1.4,[b] 1.5[c]	0.737	9.63 (1.95)	8.86 (1.12)	–
C[d]	III	activated C	TEAMS	1.7	0.693	8.64 (3.67)	7.64 (1.70)	–
A, B, and C	III	activated C, template C, and CDC	$TEABF_4$, TEAMS	1.0, 1.4, 1.5, 1.7	0.259	6.49 (2.55)	7.01 (1.87)	–
D[c]	I	CDC	$TEABF_4$	1.5	0.985	2.23 (0.30)	–	2.30 (0.14)

[a] Reference [16]. [b] Specific concentrations of 1.0 and 1.4 M were not given in reference [16], but groups A and B are tentatively assigned to 1.0 and 1.4 M, respectively (see the text). [c] Reference [8]. [d] Reference [25].

calculated the specific surface area by the nonlinear density functional theory (NLDFT) method[31] assuming slit pore shape in addition to that by the Brunauer-Emmet-Teller (BET) method.[32] We fit the second set of data normalized with the specific surface area from NLDFT and obtained $a_0 = 0.51$ Å and $\varepsilon_r = 6.72$,[12] which do not agree as well with our calculations and with the fact that the pore size is too small to accommodate solvated ions that would otherwise result in a higher dielectric constant. The normalized capacitance values for the rest of the data in this paper are based on the BET surface area. Comparing the largest capacitance in this regime with the limiting capacitance value of large pores, we find that micropores have some advantage over mesopores as indicated by Gogotsi and co-workers.[8] It is obvious that the highest capacitance value possible for micropores is determined by the size of the desolvated counterions; therefore, engineering the sizes of the electrolyte ions may further improve the energy density of nanoporous carbon supercapacitors.

There appears to be no good model for the transition region II; however, the experimental data may still be understood in light of the sizes of the desolvated or solvated ions. Data group E has higher capacitance values than group C, showing similar anomalous behavior as in group D. We speculate that data group E should be associated with EWCCs as the larger MS^- ion dictates larger pores for the formation of EWCCs. Further experiments are indispensable to clarify this point. In comparison, the data in group F are above the extrapolated dashed curve from group D, implying larger ε_r values. Pores in this region are still too small to accommodate the inner cylinder of counterions, but solvated counterions can enter pores to form EWCCs, leading to a higher ε_r value coming from the (partially removed) solvation shell. Unlike region III, concentration should not affect the capacitance in regions I and II for the absence of its effect on d.

The data in Figure 3 are based on the total capacitance of nanoporous carbon supercapacitors. In a recent experiment on microporous CDC supercapacitors with 1.5 M $TEABF_4$ in CH_3CN, Gogotsi and co-workers dissected the total capacitances into capacitance contributions of cations and anions.[10] We fit the new data for total capacitance, and the contributions from cations and anions using Equation (3) and the results are shown in Figure 4 and Table 2. Note that in Figure 4, there is a narrow pore size range that can be fit by using Equation (3). The data on the right of the fitting range have higher normalized capacitances than the extrapolation from the fit curve because the pore size is located in region II, as shown in Figure 3. The data on the left have lower normalized capacitances than the extrapolation from the fit curve, probably due to pore bottlenecks smaller than the ions or low electrical conductivity of the CDC produced at 400 °C.[8] From the fittings, the a_0 value of TEA^+ is smaller than the literature values probably because of the restricted orientation of TEA^+ inside micropores (see below). In comparison, the a_0 value of BF_4^- is larger than the literature values by approximately 0.7 Å. These discrepancies indicate that there may be some other factors that go beyond

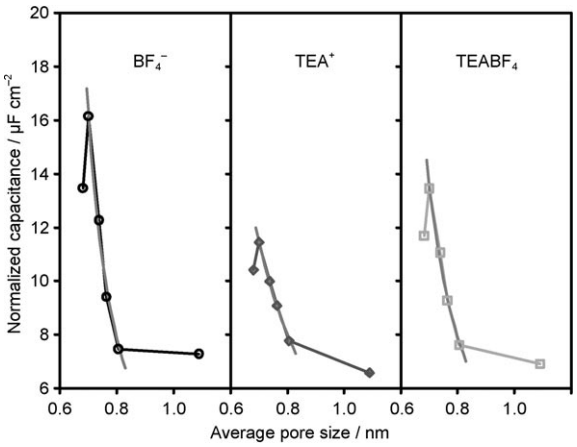

Figure 4. Experimental data of microporous CDC supercapacitors with 1.5 M $TEABF_4$ in CH_3CN (reference [10]) fit by Equation (3) for the capacitance contributions from TEA^+ (◇), BF_4^- (○) and the total capacitance (□).

Table 2. Fitting results using Equation (3) for the experimental data of total capacitance and the contributions from cations and anions with 1.5 M $TEABF_4$ in CH_3CN.[10] Numbers in parentheses are standard errors of parameters.

Capacitance contribution	R^2	ε_r	a_0 [Å]	Ionic radii [Å]
TEA^+	0.997	2.37 (0.15)	2.08 (0.07)	3.42,[a] 3.37[b]
BF_4^-	0.989	1.06 (0.11)	2.97 (0.06)	2.18,[a] 2.32[b,c]
Total	0.993	1.44 (0.12)	2.67 (0.07)	–

[a] Reference [34]. [b] Reference [35]. [c] Reference [36].

the description of our proposed model.[33] For example, the pore shapes may not be uniformly cylindrical; bottlenecks may prevent part of the pores from being accessed by ions, and therefore, the actual specific surface area is smaller than the nominal A. As a result of the different a_0 values of TEA^+ and BF_4^-, the effective a_0 obtained from total capacitance is an average value of TEA^+ and BF_4^-. Likewise, the dielectric constant obtained for the total capacitance is also an average value of TEA^+ and BF_4^-, and it is close to the vacuum value of one, showing once again the desolvation of ions before entering micropores.

Experiments with total capacitance dissected into the contributions of cations and anions are very informative. From the analysis, we obtain information regarding the effective sizes of cations and anions, respectively. Usually a supercapacitor is termed a symmetric or asymmetric capacitor, depending on whether the cathode and anode materials are the same.[2a] We can extend this terminology to supercapacitors with different sizes of electrolyte ions even though the two electrodes are made of the same carbon materials. Strictly speaking, only supercapacitors with the same electrodes and the same electrolyte ion sizes are symmetric. For such asymmetric supercapacitors with $TEABF_4$ in CH_3CN as an electrolyte, it has been found that the total capacitance is high and resistance is low when the pore size is smaller at the cathode than at the anode for $TEABF_4$ in CH_3CN.[37]

Reversing the electrodes leads to a decreased capacitance and a significantly increased resistance. Thus, a $TEABF_4$-based carbon supercapacitor with improved electrochemical properties would be one that uses carbon materials with pores adapted to the size of electrolyte ions.[6a]

DFT calculations of ionic radii: To corroborate the parameter a_0 obtained from the fits described above, we calculated the radial charge distribution of electrolyte ions enclosed in nanotubes.

First, we examine BF_4^-: The geometry optimizations were performed with B3LYP/cc-pVDZ using the NWChem suite of programs[38] for BF_4^- with T_d symmetry and two neutral "armchair" nanotubes terminated with hydrogen atoms. To simulate pores around 1 nm diameter, herein we employed a (6,6) tube with molecular formula $C_{156}H_{24}$, which has a D_{6h} symmetry and a diameter of ≈ 8 Å (labeled as a66(H)) and an (8,8) tube with molecular formula $C_{208}H_{32}$, which has a D_{8h} symmetry and a diameter of ≈ 11 Å (labeled as a88(H)). The resulting BF_4 moiety was then placed at the center of a66(H) and a88(H) tubes. To reduce computational cost, the orientation of BF_4, a66(H), and a88(H) were adjusted so that their symmetries are commensurate, leading to the highest possible symmetry C_{2v} for BF_4@a66(H) and BF_4@a88(H), in which the @ symbol indicates that BF_4 is enclosed at the center of the two tubes. Assuming rigid pores, we performed constrained optimizations for BF_4@a66(H) and BF_4@a88(H) with the geometries of the tubes and the center of the inner ions fixed. Both BF_4@a66(H) and BF_4@a88(H) are neutral, and charge transfer takes place automatically to give rise to the final charge states, as indicated by BF_4^-@a66(H)$^+$ and BF_4^-@a88(H)$^+$.

The optimized geometries of BF_4^-@a66(H)$^+$ and BF_4^-@a88(H)$^+$ were used to calculate the charge densities (CDs) of these systems and of neutral moieties BF_4, a66(H), and a88(H). The CD difference for BF_4^-@a66(H)$^+$ was then calculated by $CD(BF_4^-@a66(H)^+)-[CD(BF_4)+CD(a66(H))]$, which provided the locations of the electron and the hole.[39] This process was also carried out for BF_4^-@a88(H)$^+$. The CD difference of BF_4^-@a88(H)$^+$ is shown in Figure 5 to illustrate the charge transfer from the tube to BF_4. (The CD difference plots for other ions are available in the Supporting Information of reference [12].) The radial charge distributions of BF_4^-@a66(H)$^+$ and BF_4^-@a88(H)$^+$ (shown in Figure 6) were calculated from the CD differences within the boron-centered sphere by assuming that there is a room-temperature rotation of BF_4^- inside the pore. To test the effect of the enclosure of the a66(H) and a88(H) tubes, we also calculated the CD difference for a bare BF_4^- ion with T_d symmetry by $CD(BF_4^-)-CD(BF_4)$ and the corresponding radial charge distribution. As we can see from Figure 6, within a 3 Å radius, the curves for BF_4^-@a66(H)$^+$ and BF_4^-@a88(H)$^+$ are positive, which indicates the presence of electrons on the BF_4 moieties as a result of charge transfer. Outside the 3 Å radius, the curves are negative, which indicates the presence of holes on the tubes. In comparison, the curve for the bare BF_4^- ion is ≥ 0 as a result of the additional electron.

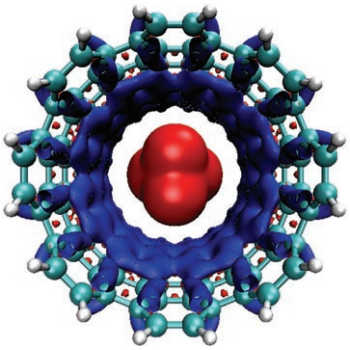

Figure 5. Charge density (CD) isosurface of BF_4^-@a88(H)$^+$ with C_{2v} symmetry calculated by $CD(BF_4^-@a88(H)^+)-[CD(BF_4)+CD(a88(H))]$ showing the locations of electron (red) and hole (blue).

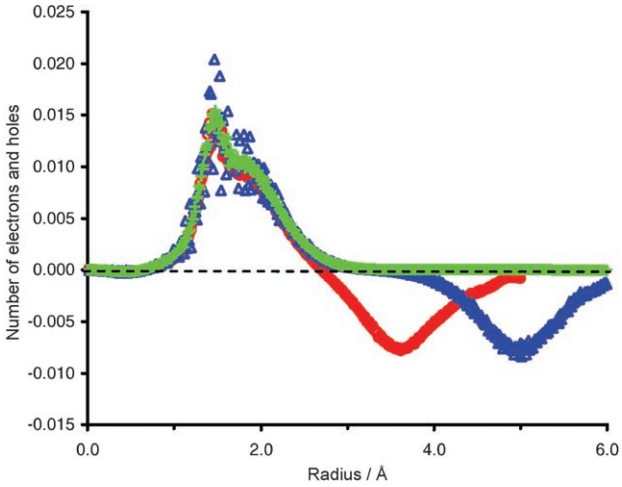

Figure 6. Radial charge distributions as a function of radius within the boron-centered sphere for BF_4^-@a66(H)$^+$ (○), BF_4^-@a88(H)$^+$ (△), and BF_4^- (+).

By integrating the radial charge distribution, we obtained the integrated number of electrons as a function of radius (Figure 7). Then we considered a_0 as the radius at which 90% of the electron is enclosed from the curves in Figure 7. The a_0 values obtained are 2.22, 2.31, and 2.31 Å for BF_4^- enclosed in a66(H) and a88(H), and for the bare ion, respectively. The estimated radius of BF_4^- is almost constant regardless of the environment and is in good agreement with the literature value of approximately 2.2–2.3 Å[34–36] and the fitting results shown in Tables 1 and 2, which supports the validity of the proposed heuristic model shown in Equation (3).

Next we turn to TEA^+. Figure 8a shows the top view of the global minimum of TEA with D_{2d} symmetry. The projection of the four terminal atoms is a square and the diagonal of the square is along the ethyl group. We assume that TEA^+ enters the pore of a66(H) with a radius 4.1 Å with its C_2' axis in alignment with the pore axis (Figure 8b) so that

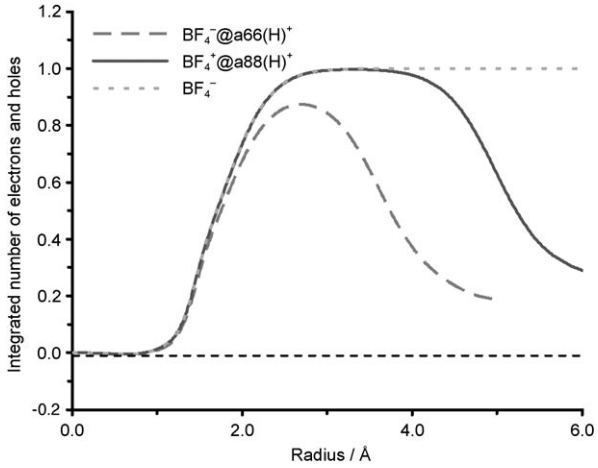

Figure 7. Integrated radial charge distribution as a function of radius within the boron-centered sphere for BF_4^-@a66(H)$^+$, BF_4^-@a88(H)$^+$, and BF_4^-. The maximum of BF_4^-@a66(H)$^+$ is ≈0.9 e because of the cancellation from the tube, whereas those of BF_4^-@a88(H)$^+$ and BF_4^- are ≈1.0 e.

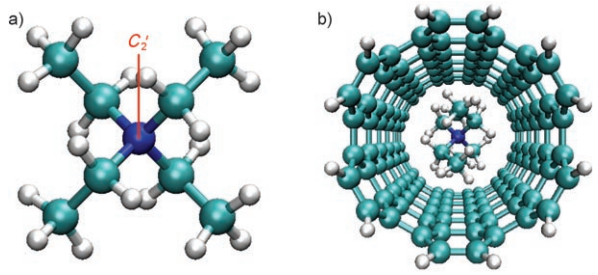

Figure 8. a) Top view of the global minimum of TEA with D_{2d} symmetry with C_2 principle axis perpendicular to the paper plane and C_2' axis lying in and b) top view of TEA$^+$@a66(H)$^-$ with the C_2' axis of TEA down in alignment with the pore axis.

TEA$^+$ would not be too close to the pore walls. The geometry of TEA@a66(H) was optimized with B3LYP/cc-pVDZ by using NWChem.[38] To reduce computational cost, the orientations of TEA and a66(H) were adjusted so that their symmetries are commensurate, leading to the highest possible symmetry of D_2. The system is neutral and charge transfer takes place automatically to give rise to TEA$^+$@a66(H)$^-$. Assuming rigid pores, we performed constrained optimization of TEA$^+$@a66(H)$^-$ with the geometries of the tube and the center of the inner ion fixed. Similar to the case of BF_4^-@a66(H)$^+$, the CD difference for TEA$^+$@a66(H)$^-$ was then calculated by CD(TEA$^+$@a66(H)$^-$)−[CD(TEA)+CD(a66(H))]. For radial charge distribution, we found by Mulliken population analysis that the positive charge is primarily located around the terminal methyl groups,[12] and therefore, the radial charge distribution was calculated within the plane that has two terminal C atoms and is perpendicular to the pore axis.

As can be seen from the radial charge distribution curve in Figure 9, within a 3 Å radius the curve is negative, which shows the presence of holes. Outside the 3 Å radius, the curve is positive, which indicates the presence of electrons on the tube. By integrating the radial charge distribution (Figure 9), we estimate that the a_0 value of TEA$^+$ is ≈2.38 Å. This is different from the literature value of 3.4 Å,[34,35] which is about the length of an ethyl group. A rough calculation of the side length of the square by trigonal geometry using the ethyl length of 3.4 Å gives an a_0 value of 2.4 Å. These calculated a_0 values agree approximately with the a_0 values in Tables 1 and 2.

For the geometry of MS$^-$ in a staggered conformation with C_{3v} symmetry, the calculation was performed in vacuum because the ion size of BF_4^- in vacuum is the same as that in an a88(H) tube. The CD difference for MS$^-$ was calculated by CD(MS$^-$)−CD(MS). Similar to TEA$^+$, MS$^-$ is assumed to enter a micropore with its C_3 principle axis down the pore axis[12] owing to the relatively large dimension along the C_3 axis. The radial charge distribution was calculated within the plane of the O atoms perpendicular to the C_3 axis at which the negative charge is mainly located according to the Mulliken population analysis. The ionic radius for MS$^-$ was then estimated from the integrated radial charge distribution and was found to be 3.13 Å. The effective a_0 value of MS$^-$ is larger than that of BF_4^- in micropores, thereby explaining the observation that data

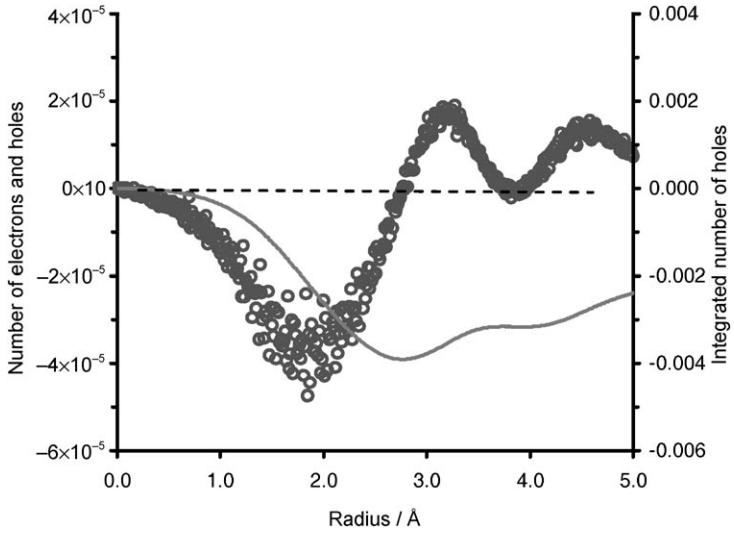

Figure 9. Differential and integrated radial charge distributions as a function of radius within the plane containing two terminal C atoms perpendicular to the pore axis for TEA$^+$@a66(H)$^-$. ○: Number of electrons and holes and ——: integrated number of holes.

group E has a larger pore size than group D (see Figure 3). We note that the TEAMS-based supercapacitors are more asymmetric than $TEABF_4$-based supercapacitors because of the larger difference in ion sizes between TEA^+ and MS^-.

Ionic liquid electrolyte: The advantage of using an ionic liquid electrolyte in supercapacitors is that a further increase of capacitor voltage can be achieved compared with organic electrolytes.[6a] Another reason to use ionic liquid electrolytes is that the electrolyte ions do not have any solvation shells due to the absence of solvent molecules. The bare ions allow one to discern the ion sieving properties of porous carbon materials without the interference of solvent molecules.[40]

In a recent experiment on CDC supercapacitors,[11] Simon and co-workers employed a 1-ethyl-3-methylimidazolium bis(trifluoromethanesulfonyl)imide (EMI-TFSI) ionic liquid as an electrolyte and also found the increasing capacitance with decreasing subnanometer pore size, exactly as that shown in group D of Figure 3. Thus, the explanation of Gogotsi and co-workers for the anomalous increase in capacitance of CDC supercapacitors by a desolvation of electrolyte ions entering subnanometer pores[8] is verified. Herein we present our analysis of the experimental data to show the validity of the EWCC model for ionic liquid electrolytes (Figure 10).

As can be seen in Figure 10, we were able to fit the data in the middle pore range to give $\varepsilon_r = 1.12$ and $a_0 = 2.91$ Å. The value of ε_r is very close to the vacuum value of one, which shows the absence of solvents. The a_0 value compares well with the ions size of EMI^+ and $TFSI^-$ (Table 3). Both EMI^+ and $TFSI^-$ can be approximated as rectangular shape with dimensions of 4.3×7.6 and 2.9×7.9 Å^2, respectively.[11] The ionic radii along the short and long dimensions are 2.15 and 3.80 Å for EMI^+, respectively, and are 1.45 and 3.85 Å for $TFSI^-$, respectively. It appears that the a_0 value of 2.91 Å from the fitting is the average value of the ionic radii along the short and long dimensions, which suggests room-temperature rotation of ions inside the pores. Similar to what has been observed for $TEABF_4/CH_3CN$ in CDC micropores (Figure 4), there is a decrease of specific capacitances with pores smaller than 0.7 nm. This was ascribed to an increased portion of pores that are too small to be accessed by the electrolyte ions.[11] For pores above 0.8 nm, the capacitance deviates from the EWCC model. It would be interesting to perform some experiments with mesopores to find out if there is a slight increase in capacitance with increasing pore size in the case of ionic liquid electrolyte the same as in the organic electrolyte (region III in Figure 3), and if the mesoporous supercapacitors can be described by the EDCC model.

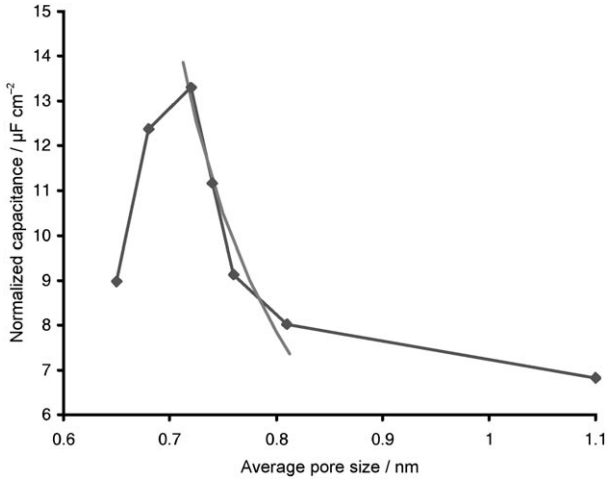

Figure 10. Experimental data (◆) of microporous CDC supercapacitors using 1-ethyl-3-methylimidazolium-bis(trifluoromethanesulfonyl)imide ionic liquid (EMI-TFSI) as the electrolyte[11] fit by Equation (3) for the total capacitance.

Aqueous electrolytes of H_2SO_4 and KOH: In addition to organic and ionic liquid electrolytes, we also found from an extended literature survey that the anomalous increase in capacitance also manifests in aqueous solutions. Below we present our analyses of available experimental data with H_2SO_4 and KOH electrolytes in both micropore and mesopore regimes. The fitting results are tabulated in Table 3.

For the 1 M aqueous H_2SO_4electrolyte, in the mesopore regime (region II in Figure 11), the capacitance values show a slight increase with increasing pore size. Fitting by using EDCC model [Eq. (2b)] yields a rather large ε_r, which can be ascribed to the solvation shell of water molecules around the electrolyte ions. The double layer is about 10 Å in thickness. In the micropore regime (region I), experimental data were obtained for three kinds of carbon materials, including TiC-CDC, Zr-CDC, and activated C. It seems that the anomalous increase in capacitance in micropores is independent of the preparation methods of carbon materials. Fitting in this regime by using the EWCC model produces a rather large ε_r, indicating that the solutes are hydrated by water molecules, unlike the case of organic electrolytes

Table 3. Fitting results for the experimental data for diverse carbon materials with micropores and mesopores and for diverse electrolytes using Equations (3) and (2b) compared with ion sizes in literature. Numbers in parentheses are standard errors of parameters.

Pores	Carbon materials	Electrolytes	R^2	ε_r	d [Å]	a_0 [Å]	Ionic radii [Å]	
micro	CDC[a]	EMI-TFSI	0.944	1.12 (0.26)	–	2.91 (0.16)	EMI^+: 2.15,[a,b] 3.80[a,c]	$TFSI^-$: 1.45,[a,b] 3.85 [a,c]
micro	CDC,[d] activated C[e]	H_2SO_4 (1 M)	0.889	27.1 (18.7)	–	0.05 (0.17)	H^+: 0.28[g]	SO_4^{2-}: 2.40,[h] 2.58 [i]
meso	template C[f]		0.328	17.4 (6.3)	9.77 (1.92)	–		
micro	activated C[e]	KOH (6 M)	0.921	7.76 (3.06)	–	1.64 (0.83)	K^+: 1.38[h]	OH^-: 1.33[h,j]
meso	activated C[j]		0.618	13.4 (3.2)	6.72 (1.03)	–		

[a] Reference [11]. [b] Along the short dimension. [c] Along the long dimension. [d] Reference [41]. [e] Reference [42]. [f] Reference [16]. [g] Reference [43]. [h] Reference [35]. [i] Reference [36]. [j] Reference [44].

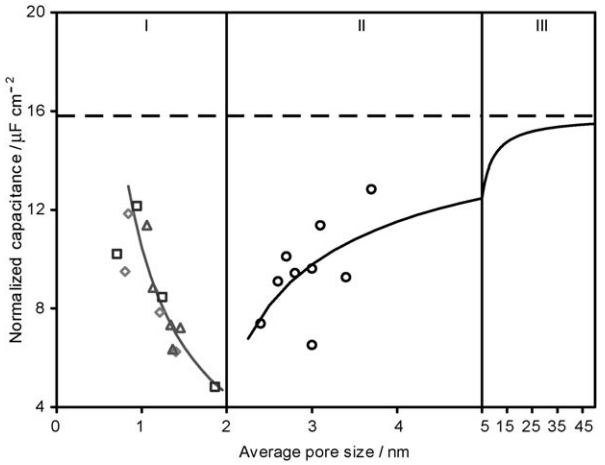

Figure 11. Experimental data of supercapacitors with diverse microporous and mesoporous carbon materials in a 1 M aqueous H_2SO_4 electrolyte fit by Equation (3) and (2b) for region I and II, respectively. The extrapolation of the curve in region II into region III approaches the broken line calculated by Equation (1b) using the same parameters as obtained from region II. Note in region I, the two leftmost data points are excluded from the fitting. ◇: ZrC–CDC, □: TiC–CDC, △: activated carbon material, and ○: template carbon material.

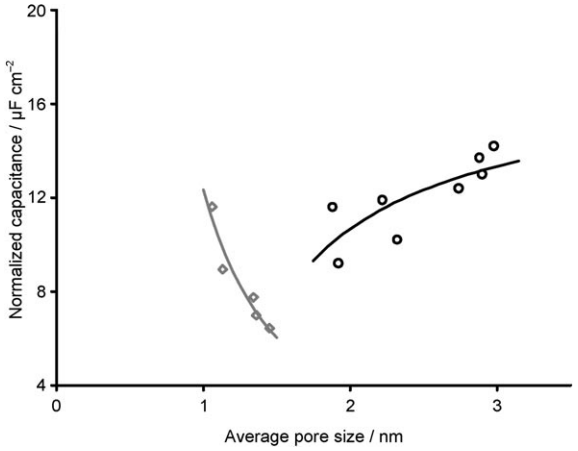

Figure 12. Experimental data of supercapacitors with activated carbon electrode materials in a 6 M aqueous KOH electrolyte fit by Equation (3) and (2b) for micropores (◇) and mesopores (○), respectively.

(Table 1). The a_0 value of (0.05 ± 0.17) Å appears to be in good agreement with the ionic radius of proton. (Note that a_0 is determined by the extent of electron density around the ions; and therefore, a_0 would remain more or less constant with or without the solvation shell.) Protons are prone to hydration because of the relatively strong hydrogen-bonding interactions with water molecules. Hydrated protons $H^+(H_2O)_n$ have long been a subject of theoretical studies.[45,46] Other observations to support the fact that the electrolyte ions are solvated in micropore regime are 1) there is no transition region between micropore regime and mesopore regime (cf. region II in Figure 3), and 2) the capacitance drops at a larger micropore size ($\approx$1 nm) compared with the cases of organic and ionic liquid electrolytes ($\approx$0.7 nm), even though both proton and SO_4^{2-} are smaller than the ions considered before. It is not clear why there is no sign of the anion SO_4^{2-} from the fitting of micropore data. An experiment would be helpful in clarifying this problem with the total capacitance dissected into the respective contributions from proton and SO_4^{2-}. Extrapolation of the curve in region II into region III shows that the curve asymptotically approaches the broken line calculated by Equation (1b) using the same parameters ε_r and d as in region II. The broken line represents the limiting value of normalized capacitance for large pores at a concentration of 1 M aqueous H_2SO_4. Comparing the limiting values in region III and region I, one can see from Figure 11 that the limiting value of microporous capacitance is below that of the macropores. This is different from the case of organic electrolytes (Figure 3), as a result of the larger hydrated ions in micropores with aqueous H_2SO_4 electrolyte.

For the 6 M aqueous KOH electrolyte, once again we show that the EDCC and EWCC models are applicable to the mesopore and micropore regimes, respectively (Figure 12). The fitting of micropores gives an $a_0 = (1.64 \pm 0.83)$ Å, in good agreement with the ion sizes of K^+ and OH^- (Table 3). It is clear from the fitting results that the electrolyte ions are hydrated by water molecules in micropores, the same as the 1 M aqueous H_2SO_4 electrolyte. There is experimental[40] and theoretical evidence[47] showing that alkaline ions are solvated in micropores with pore size <1 nm. For mesoporous carbon materials, we selected only eight data points from reference [44] because the EDCC and/or EWCC model is only applicable to unimodal pores. The pore size distributions of these carbon materials are approximately unimodal, as can be seen from Figure 2 in reference [44]. We excluded four other carbon materials with labels LA/CaCo, LA/CaFe, LA/CaFedem, and SA/S/CaFe, which have pronounced multimodal pore size distributions. The capacitance data of these four carbon materials do not form a trend with the rest of the data. With these four carbon materials excluded, we were able to fit the experimental data to give an acceptable R^2 value of 0.618.

Kinetic process of solvation/desolvation: Usually it is found that capacitance of mesoporous carbon materials is reduced at large discharging current densities, probably because of the solute diffusion process. Such behavior of reduced capacitance also exists for microporous carbon materials.[8] However, the reduced capacitance is more pronounced for microporous carbon materials than mesoporous carbon materials. Tamai et al.[48] found that, at smaller discharge currents, the capacitances of mesoporous and microporous carbon materials in $TEABF_4$ organic electrolyte are in one data group, but are separated into two data groups at larger discharge current, in which the capacitances of microporous carbon materials are reduced by a larger degree than those of mesoporous carbon materials. This difference should be ascribed to the following solvation/desolvation process of TEA^+ and BF_4^-, which plays a significant role only for micropores [Eq. (4)].

$$I^{\pm}+nS \rightleftharpoons I^{\pm}S_n \quad (4)$$

in which I and S stand for ions and solvent molecules, respectively. A negative Gibbs free energy change favors the ion solvation process. The desolvation process contributes to the equivalent series resistance in microporous carbon materials, but not in mesoporous carbon materials.

Temperature should also play a role in capacitance through Equation (4). Raising the temperature may facilitate the desolvation process owing to a negative entropy change according to $\Delta G=\Delta H-T\Delta S$. Leis et al.[49] found that, for carbon materials in triethylmethylammonium tetrafluoroborate ($TEMABF_4$) electrolyte with pores smaller than 11 Å, the power density increases with temperature; for others with only pores larger than 11 Å, the power density is almost independent of temperature. The critical pore size of 11 Å (or 10 Å in Figures 3, 4, and 10) is characteristic of EWCCs with $TEMABF_4$ or $TEABF_4$ as the electrolyte. Note that $TEMA^+$ differs from TEA^+ by only one methyl group, and therefore, the ionic radii of these two ions are comparable. For EDCCs, the effect of temperature on capacitance might be cancelled out owing to its reverse effects on d and solvent viscosity.

For ionic liquid and aqueous electrolytes, as can be seen from Figures 10 to 12 and Table 3, no desolvation process in the micropore regime is involved. Therefore, it is expected that the deterioration of microporous carbon capacitance at larger discharging current densities is less pronounced than in organic electrolytes. We suggest that experiments be performed to test whether capacitances of microporous carbon materials are reduced by a comparable degree to mesoporous carbon materials at large discharging current.

Nanoporous carbon materials with multimodal pore size distribution: With all pore regimes covered, we comment on the application of Equations (2) and (3). As noted previously, the EDCC and/or EWCC model is only applicable to unimodal pores. Strictly speaking, among the materials discussed above, only the CDCs have a unimodal pore size distribution because of their very narrow pore size distribution.[8] For the experimental data of other carbon materials, Equations (2b) and (3) alone do not work as well, as can be seen from the wide range of R^2 from 0.2 to 0.9.

For pores with a multimodal pore size distribution, one should include the contributions to capacitance from macro-, meso-, and micropores. The complete model should be that shown in Equation (5):

$$C=\sum_i \frac{\varepsilon_{r,micro}\varepsilon_0 A_{i,micro}}{b_i \ln(b_i/a_0)}+\sum_j \frac{\varepsilon_{r,meso}\varepsilon_0 A_{j,meso}}{b_j \ln[b_j/(b_j-d)]}+\sum_k \frac{\varepsilon_{r,macro}\varepsilon_0 A_{k,macro}}{d} \quad (5)$$

In cases in which macropores are only a small portion of the pores and the pore size distribution of micropores and mesopores is narrow, yielding bimodal pores, this approximately becomes Equation (6):

$$C=\frac{\varepsilon_{r,micro}\varepsilon_0 A_{micro}}{b_{micro}\ln(b_{micro}/a_0)}+\frac{\varepsilon_{r,meso}\varepsilon_0 A_{meso}}{b_{meso}\ln[b_{meso}/(b_{meso}-d)]} \quad (6)$$

A modified version of Equation (6) has been employed by Shi[14a] for carbon supercapacitors with bimodal pores producing a good linear relationship between C/A_{meso} and A_{micro}/A_{meso}. This, however, should work well only when the areas (A_{micro} and A_{meso}) and their ratio are allowed to change while the pore sizes are fixed to give a constant slope and intercept.[41]

Endohedral versus exohedral supercapacitors: In addition to nanoporous carbon materials, other carbon materials have also been experimentally studied for electrode materials of supercapacitors, such as single-walled nanotubes (SWNTs), multi-walled nanotubes (MWNTs),[50] and carbon nanofibers or nanowires.[51] In sharp contrast to nanoporous carbon materials, for which counterions enter pores to form endohedral EDCCs and/or EWCCs, for nanotubes with end caps and solid nanowires, counterions reside on the outside of the surfaces, which leads to exohedral EDCCs (Figure 13).

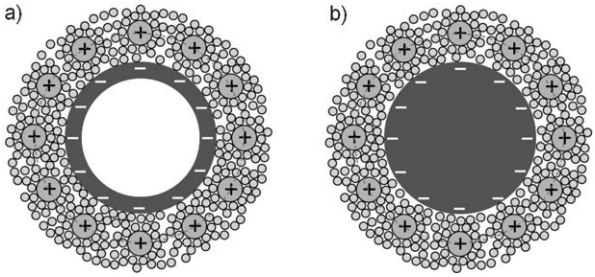

Figure 13. Exohedral-type EDCC with counterions forming an outer cylinder on a) a negatively charged nanotube (hollow) and b) nanowire (solid).

(An EWCC is not possible.) For nanowires with diameters in the order of 100 nm, the EDLC model is probably still valid. For carbon nanotubes, the EDLC model is usually used for the discussion of electrochemical properties.[50a] However, on the basis of the insight obtained from the nanoporous carbon materials, the EDCC model should be the reasonable choice for modeling exohedral supercapacitors based on carbon nanotubes. Note that Equation (2) is not applicable unless the diameter sizes of these materials are strictly controlled to be monodispersed. It is challenging to model nanotubes, mainly because nanotubes are quite difficult to purify and samples are typically made up of a complicated mixture that contains various types of tubes. SWNTs could have diverse properties that arise from zigzag, armchair, and chiral or helical structures, let alone MWNTs. Even for just a single type of tube, the dimension change as a function of charge injection[52] may cause the variation of the specific surface area of electrode materials during charging/discharging. In spite of that, the advantage of exohedral supercapacitors is that counterions have easy access to the

carbon/electrolyte interface without having to enter the pores, which could increase the equivalent series resistance. Therefore, it is likely that exohedral supercapacitors have more rapid charging/discharging properties than endohedral ones.

Conclusion

In response to the latest experimental developments in nanoporous carbon supercapacitors as a novel type of energy-storage device, we have proposed a heuristic theoretical model that takes pore curvature into account to replace the EDLC model for a traditional parallel-plate capacitor. The carbon particles of the supercapacitor electrodes are in the order of micrometers in size and each particle contains a large amount of pores with diameters in the order of nanometers. The large specific surface area of carbon materials includes a relatively small contribution from the surface area of the particles and a major contribution from the pores inside the particles. For mesopores, counterions enter mesoporous carbon materials and approach the pore wall to form an EDCC; for micropores, solvated/desolvated counterions line up along the pore axis to form an EWCC. The EDCC model can be reduced naturally to the EDLC model when the pores are large enough so that the pore curvature is no longer significant and can be approximated to be planar. We have presented DFT calculations and detailed analyses of available experimental data in various pore regimes for diverse carbon materials, including activated carbon materials, template carbon materials, and the novel carbide-derived carbon materials, which show significant effects of pore curvature on the supercapacitor properties of nanoporous carbon materials. It can be concluded that the EDCC/EWCC model is valid regardless of what type of carbon materials are used for electrode-active materials and is universal to carbon supercapacitors with diverse electrolytes of various concentrations. Thus, supercapacitor properties can be correlated with pore size, specific surface area, Debye length, electrolyte concentration, and dielectric constant, as well as solute ion size through the EDCC/EWCC model, which may lend support for the systematic optimization of the properties of carbon supercapacitors through experiments.

The EWCC model also provides crucial insight into the behavior of electrolyte ions inside nanoconfined spaces. Fitting the results of experimental data indicates that organic ions tend to be desolvated before entering subnanometer pores, whereas aqueous electrolyte ions can retain their hydration shell in subnanometer pores. In addition, it appears that some electrolyte ions undergo room-temperature rotations inside micropores and the orientations of some other electrolytes ions in micropores are restricted. All of the experiments cited herein were performed near room temperature. It would be interesting to find out whether the room-temperature rotation of electrolyte ions can be frozen out at low temperature, not from a practical, but a fundamental point of view. Such information can be theoretically probed by using the EWCC model and DFT calculations of ionic radii based on the orientation of ions inside micropores. The knowledge acquired can also be beneficial for understanding ion transfer in ion channels of cells. A challenge is that the electrolyte solvents may become frozen at low temperature before the rotation of electrolyte ions can be studied.

Associated with the understanding given above, other conclusions can be drawn: 1) The experiments by Gogotsi and co-workers[10] with total capacitance dissected into the contributions of cations and anions are very informative in that the EDCC/EWCC model can be applied separately to the cations and anions, which produces different sets of electrochemical parameters. 2) As suggested by Frackowiak,[6a] the capacitance properties of asymmetric nanoporous carbon supercapacitors with electrolytes of different ion sizes can be improved by using carbon materials with pores adapted to the size of the electrolyte ions. 3) Porous carbon materials with various pore sizes may be combined to achieve both high energy densities due to micropores and high power densities due to mesopores. 4) For aqueous electrolytes considered herein, there is no gain of energy densities in microporous carbon materials compared with mesopores for supercapacitors as a result of the larger hydrated ions.

Acknowledgements

We gratefully acknowledge support from the Laboratory Directed Research and Development Program of Oak Ridge National Laboratory (ORNL) and from the Division of Materials Sciences and Engineering, U.S. Department of Energy under Contract No. DEAC05-00OR22725 with UT-Battelle, LLC at ORNL. We thank Prof. Dr. Y. Gogotsi and his group for providing the experimental data for reference [10]. We are also indebted to Prof. Dr. M. Kertesz for helpful discussions on charge injection from molecules on the outer surface of nanotubes to nanotubes and the resulting dimensional and surface area changes.

[1] B. E. Conway, *Electrochemical Supercapacitors: Scientific Fundamentals and Technological Applications*, Kluwer Academic/Plenum, New York, **1999**.
[2] For reviews, see: a) M. Winter, R. J. Brodd, *Chem. Rev.* **2004**, *104*, 4245; b) A. Burke, *J. Power Sources* **2000**, *91*, 37; c) R. Kötz, M. Carlen, *Electrochim. Acta* **2000**, *45*, 2483; d) S. Sarangapani, B. V. Tilak, C.-P. Chen, *J. Electrochem. Soc.* **1996**, *143*, 3791.
[3] Faradaic process does exist in electrochemical capacitors utilizing pseudocapacitances, for example, in the most investigated RuO_2–aqueous H_2SO_4 system.
[4] A. G. Pandolfo, A. F. Hollenkamp, *J. Power Sources* **2006**, *157*, 11.
[5] *New Carbon Based Materials for Electrochemical Energy Storage Systems: Batteries, Supercapacitors and Fuel Cells* (Eds.: I. V. Barsukov, C. S. Johnson, J. E. Doninger, V. Z. Barsukov), Springer, Dordrecht, The Netherlands, **2006**.
[6] For reviews, see: a) E. Frackowiak, *Phys. Chem. Chem. Phys.* **2007**, *9*, 1774; b) A. S. Aricò, P. Bruce, B. Scrosati, J.-M. Tarascon, W. van Schalkwijk, *Nat. Mater.* **2005**, *4*, 366.
[7] Y. Gogotsi, A. Nikitin, H. Ye, W. Zhou, J. E. Fischer, B. Yi, H. C. Foley, M. W. Barsoum, *Nat. Mater.* **2003**, *2*, 591.
[8] J. Chmiola, G. Yushin, Y. Gogotsi, C. Portet, P. Simon, P. L. Taberna, *Science* **2006**, *313*, 1760.

[9] Unimodal pores have a uniform (and therefore narrow) pore size distribution, in contrast with multimodal pores in which there are different pore sizes.
[10] J. Chmiola, C. Largeot, P.-L. Taberna, P. Simon, Y. Gogotsi, *Angew. Chem.* **2008**, *120*, 3440; *Angew. Chem. Int. Ed.* **2008**, *47*, 3392.
[11] C. Largeot, C. Portet, J. Chmiola, P.-L. Taberna, Y. Gogotsi, P. Simon, *J. Am. Chem. Soc.* **2008**, *130*, 2730.
[12] J. Huang, B. G. Sumpter, V. Meunier, *Angew. Chem.* **2008**, *120*, 530; *Angew. Chem. Int. Ed.* **2008**, *47*, 520.
[13] a) D. Lozano-Castelló, D. Cazorla-Amorós, A. Linares-Solano, S. Shiraishi, H. Kurihara, A. Oya, *Carbon* **2003**, *41*, 1765; b) C. Lin, J. A. Ritter, B. N. Popov, *J. Electrochem. Soc.* **1999**, *146*, 3639; c) T. Morimoto, K. Hiratsuka, Y. Sanada, K. Kurihara, *J. Power Sources* **1996**, *60*, 239.
[14] a) H. Shi, *Electrochim. Acta* **1996**, *41*, 1633; b) D. Qu, H. Shi, *J. Power Sources* **1998**, *74*, 99.
[15] M. Endo, Y. J. Kim, T. Takeda, T. Maeda, T. Hayashi, K. Koshiba, H. Hara, M. S. Dresselhaus, *J. Electrochem. Soc.* **2001**, *148*, A1135.
[16] C. Vix-Guterl, E. Frackowiak, K. Jurewicz, M. Friebe, J. Parmentier, F. Béguin, *Carbon* **2005**, *43*, 1293.
[17] E. Frackowiak, G. Lota, J. Machnikowski, C. Vix-Guterl, F. Béguin, *Electrochim. Acta* **2006**, *51*, 2209.
[18] K. S. W. Sing, D. H. Everett, R. A. W. Haul, L. Moscou, R. A. Pierotti, J. RouquQrol, T. Siemieniewska, *Pure Appl. Chem.* **1985**, *57*, 603.
[19] a) G. Q. Lu, X. S. Zhao in *Nanoporous Materials: Science and Engineering* (Eds.: G. Q., Lu, X. S. Zhao), World Scientific, Singapore, **2004**, Chapter 1; b) D. H. Everett, J. C. Powl, *J. Chem. Soc. Faraday Trans. 1* **1976**, *72*, 619.
[20] a) C. Liang, K. Hong, G. A. Guiochon, J. W. Mays, S. Dai, *Angew. Chem.* **2004**, *116*, 5909; *Angew. Chem. Int. Ed.* **2004**, *43*, 5785; b) C. Liang, S. Dai, *J. Am. Chem. Soc.* **2006**, *128*, 5316.
[21] a) S. J. Gregg, K. S. W. Sing, *Adsorption, Surface Area and Porosity*, Academic, New York, **1967**, Chapter 3; b) R. Evans, U. M. B. Marconi, P. Tarazona, *J. Chem. Soc. Faraday Trans. 2* **1986**, *82*, 1763.
[22] a) R. de Levie, *Electrochim. Acta* **1963**, *8*, 751; b) M. Itagaki, S. Suzuki, I. Shitanda, K. Watanabe, H. Nakazawa, *J. Power Sources* **2007**, *164*, 415; c) J. H. Jang, S. M. Oh, *J. Electrochem. Soc.* **2004**, *151*, A571.
[23] P. A. Tipler, *Physics*, Worth, New York, **1976**, p. 769.
[24] Fitting is performed by using the OriginPro 7.5 program.
[25] J. Gamby, P. L. Taberna, P. Simon, J. F. Fauvarque, M. Chesneau, *J. Power Sources* **2001**, *101*, 109.
[26] E. Lust, A. JRnes, T. PRrn, P. Nigu, *J. Solid State Electrochem.* **2004**, *8*, 224.
[27] C.-M. Yang, Y.-J. Kim, M. Endo, H. Kanoh, M. Yudasaka, S. Iijima, K. Kaneko, *J. Am. Chem. Soc.* **2007**, *129*, 20.
[28] J.-F. Côté, D. Brouillette, J. E. Desnoyers, J.-F. Rouleau, J.-M. St-Arnaud, G. Perron, *J. Solution Chem.* **1996**, *25*, 1163.
[29] a) B. E. Conway, J. O'M. Bockris, I. A. Ammar, *Trans. Faraday Soc.* **1951**, *47*, 756; b) L. S. Palmer, A. Cunliffe, J. M. Hough, *Nature* **1952**, *170*, 796; c) J. Dzubiella, J.-P. Hansen, *J. Chem. Phys.* **2005**, *122*, 234706.
[30] A. B. Fuertes, G. Lota, T. A. Centento, E. Frackowiak, *Electrochim. Acta* **2005**, *50*, 2799.
[31] P . I. Ravikovitch, A. Neimark, *Colloids Surf. A* **2001**, *187–188*, 11.
[32] S. Brunauer, P. Emmett, E. Teller, *J. Am. Chem. Soc.* **1938**, *60*, 309.
[33] Y. Gogotsi, private communication.
[34] M. Ue, *J. Electrochem. Soc.* **1994**, *141*, 3336.
[35] Y. Marcus, *Biophys. Chem.* **1994**, *51*, 111.
[36] H. D. B. Jenkins, K. P. Thakur, *J. Chem. Educ.* **1979**, *56*, 576.
[37] M. Okamura, JEOL, US 6064562, **2000**.
[38] NWChem, A Computational Chemistry Package for Parallel Computers, Version 4.7, E. Apra, T. L. Windus, T. P. Straatsma, E. J. Bylaska, W. de Jong, S. Hirata, M. Valiev, M. T. Hackler, L. Pollack, K. Kowalski, R. J. Harrison, M. Dupuis, D. M. A. Smith, J. Nieplocha, V. Tipparaju, M. Krishnan, A. A. Auer, E. Brown, G. I. Cisneros, G. Fann, H. Fruchtl, J. Garza, K. Hirao, R. Kendall, J. A. Nichols, K. Tsemekhman, K. Wolinski, J. Anchell, D. Bernholdt, P. Borowski, T. Clark, D. Clerc, H. Dachsel, M. Deegan, K. Dyall, D. Elwood, E. Glendening, M. Gutowski, A. Hess, J. Jaffe, B. Johnson, J. Ju, R. Kobayashi, R. Kutteh, Z. Lin, R. Littlefield, X. Long, B. Meng, T. Nakajima, S. Niu, M. Rosing, G. Sandrone, M. Stave, H. Taylor, G. Thomas, J. van Lenthe, A. Wong, Z. Zhang, Pacific Northwest National Laboratory, Richland, WA (USA), **2005**.
[39] V. Meunier, B. G. Sumpter, *J. Chem. Phys.* **2005**, *123*, 024705.
[40] G. Salitra, A. Soffer, L. Eliad, Y. Cohen, D. Aurbach, *J. Electrochem. Soc.* **2000**, *147*, 2486.
[41] J. Chmiola, G. Yushin, R. Dash, Y. Gogotsi, *J. Power Sources* **2006**, *158*, 765.
[42] G. Lota, T. A. Centeno, E. Frackowiak, F. Stoechkli, *Electrochim. Acta* **2008**, *53*, 2210.
[43] a) R. Heyrovska, *Chem. Phys. Lett.* **2006**, *432*, 348; b) R. Heyrovska, *Mol. Phys.* **2005**, *103*, 877.
[44] G. Gryglewicz, J. Machnikowski, E. Lorenc-Grabowska, G. Lota, E. Frackowiak, *Electrochim. Acta* **2005**, *50*, 1197.
[45] a) M. D. Newton, S. Ehrenson, *J. Am. Chem. Soc.* **1971**, *93*, 4971; b) M. D. Newton, *J. Chem. Phys.* **1977**, *67*, 5535.
[46] a) R. E. Kozack, P. C. Jordan, *J. Chem. Phys.* **1992**, *96*, 3131; b) L. I. Yeh, M. Okumura, J. D. Meyers, J. M. Price, Y. T. Lee, *J. Chem. Phys.* **1989**, *91*, 7319.
[47] a) M. Carrillo-Tripp, H. Saint-Martin, I. Ortega-Blake, *Phys. Rev. Lett.* **2004**, *93*, 168104; b) R. M. Lynden-Bell, J. C. Rasaiah, *J. Chem. Phys.* **1996**, *105*, 9266.
[48] See Figures 4–6 in H. Tamai, M. Kouzu, M. Morita, H. Yasuda, *Electrochem. Solid-State Lett.* **2003**, *6*, A214.
[49] J. Leis, M. Arulepp, A. Kuura, M. Lätt, E. Lust, *Carbon* **2006**, *44*, 2122.
[50] a) E. Frackowiak, R. Béguin, *Carbon* **2002**, *40*, 1775; b) C. Du, J. Yeh, N. Pan, *Nanotechnology* **2005**, *16*, 350; c) R. H. Baughman, A. A. Zakhidov, W. A. de Heer, *Science* **2002**, *297*, 787; d) C. Niu, E. K. Sichel, R. Hoch, D. Moy, H. Tennent, *Appl. Phys. Lett.* **1997**, *70*, 1480; e) J. H. Chen, W. Z. Li, D. Z. Wang, S. X. Yang, J. G. Wen, Z. F. Ren, *Carbon* **2002**, *40*, 1193; f) Q.-L. Chen, K.-H. Xue, W. Shen, F.-F. Tao, S.-Y. Yin, W. Xu, *Electrochim. Acta* **2004**, *49*, 4157; g) C.-Y. Liu, A. J. Bard, F. Wudl, I. Weitz, J. R. Heath, *Electrochem. Solid-State Lett.* **1999**, *2*, 577.
[51] a) Q. Bao, S. Bao, C. M. Li, X. Qi, C. Pan, J. Zang, Z. Lu, Y. Li, D. Y. Tang, S. Zhang, K. Lian, *J. Phys. Chem. C* **2008**, *112*, 3612; b) C. Kim, K.-S. Yang, W.-J. Lee, *Electrochem. Solid-State Lett.* **2004**, *7*, A397.
[52] a) R. H. Baughman, C. Cui, A. A. Zakhidov, Z. Iqbal, J. N. Barisci, G. M. Spinks, G. G. Wallace, A. Mazzoldi, D. D. Rossi, A. G. Rinzler, O. Jaschinski, S. Roth, M. Kertesz, *Science* **1999**, *284*, 1340; b) G. Sun, J. Kurti, M. Kertesz, R. H. Baughman, *J. Am. Chem. Soc.* **2002**, *124*, 15076.

Received: April 3, 2008
Published online: June 24, 2008

